A scalable robust microporous Al-MOF for post-combustion carbon capture

Bingbing Chen, Dong Fan, Rosana Pinto, Iurii Dovgaliuk, Shyamapada Nandi, Debanjan Chakraborty, Nicolas Heymans, Guy de Weireld, Farid Nouar, Guillaume Maurin, et al.

A scalable robust microporous Al-MOF for post-combustion carbon capture

Bingbing Chen,[1] Dong Fan,[2] Rosana V. Pinto,[1,8] Iurii Dovgaliuk,[1] Shyamapada Nandi,[1] Debanjan Chakraborty,[1] Nuria García-Moncada,[3] Alexandre Vimont,[3] Charles J. McMonagle,[4] Marta Bordonhos,[5,6] Abeer Al Mohtar,[5] Ieuan Cornu,[7] Pierre Florian,[7] Nicolas Heymans,[8] Marco Daturi,[3] Guy De Weireld,[8] Moisés Pinto,[5] Farid Nouar,[1] Guillaume Maurin,[2] Georges Mouchaham[1]* and Christian Serre[1]*.*

[1] Institut des Matériaux Poreux de Paris, Ecole Normale Supérieure, ESPCI Paris, CNRS, PSL University, 75005 Paris, France.

[2] ICGM, Univ. Montpellier, CNRS, ENSCM, 34293 Montpellier, France.

[3] Normandie Université, ENSICAEN, UNICAEN, CNRS, Laboratoire Catalyse et Spectrochimie, 14000 Caen, France.

[4] Swiss–Norwegian Beamlines, European Synchrotron Radiation Facility, 71 Avenue des Martyrs, 38000 Grenoble, France.

[5] CERENA, Departamento de Engenharia Química, Instituto Superior Técnico, Universidade de Lisboa, 1049-001 Lisboa, Portugal.

[6] CICECO – Aveiro Institute of Materials, Department of Chemistry, University of Aveiro, Campus Universitário de Santiago, 3810-193 Aveiro, Portugal.

[7] Centre National de la Recherche Scientifique (CNRS), UPR3079 CEMHTI, Université d'Orléans, 1D Av. Recherche Scientifique, CEDEX 2, 45071 Orléans, France.

[8] Service de Thermodynamique et de Physique Mathématique, Faculté Polytechnique, Université de Mons, 7000 Mons, Belgium.

Emails: guillaume.maurin1@umontpellier.fr; georges.mouchaham@ens.psl.eu; christian.serre@ens.psl.eu

Keywords: MOFs, CO_2, CCS, scale-up, shaping, techno-economic analysis

Abstract

Herein we report on a robust microporous aluminum tetracarboxylate framework, MIL-120(Al)-AP, (MIL, AP: Institute Lavoisier and Ambient Pressure synthesis, respectively), which exhibits high CO_2 uptake (1.9 mmol g^{-1} at 0.1 bar, 298 K). *In situ* Synchrotron X-ray diffraction measurements together with Monte Carlo simulations reveal that this structure offers a favorable CO_2 capture configuration with the pores being decorated with a high density of μ_2-OH groups and accessible aromatic rings. Meanwhile, based on calculations and experimental evidences, moderate host-guest interactions Q_{st} (CO_2) value of MIL-120(Al)-AP (~40 kJ mol^{-1}) is deduced, suggesting a relatively low energy penalty for full regeneration. Moreover, an environmentally friendly ambient pressure green route, relying on inexpensive raw materials, is developed to prepare MIL-120(Al)-AP at the kilogram scale with a high yield while the MOF is further shaped with inorganic binders as millimeter-sized mechanically stable beads. First evidences of its efficient CO_2/N_2 separation ability are validated by breakthrough experiments while IR *operando* experiments indicate a kinetically favorable CO_2 adsorption over water. Finally, a techno-economic analysis gives an estimated production cost of about 13 $/kg, significantly lower than for other benchmark MOFs. These advancements make MIL-120(Al)-AP an excellent candidate as an adsorbent for industrial scale CO_2 capture processes.

1. Introduction

Carbon capture, utilization and storage (CCUS) is envisioned to significantly tackle increasing levels of atmospheric CO_2 achieving the prevention of global warming.[1] Among the current potential carbon capture technologies, post-combustion capture of flue gas emitted from power plants and carbon-intensive industries as steel or cement production is considered as a feasible and economically viable process, as it might be potentially retrofitted to the existing fleet of coal-fired power stations or industrial plants.[2] So far, aqueous amine solution through a combination of chemical and physical absorption affinity with CO_2 molecule is the most applicable and mature technology for CO_2 capture.[3] However, it raises important environmental issues as well as a high energy penalty, on average 15-20% but up to 80% of total thermal energy consumption for a coal-fired power plants, in the worst case.[4] Physisorptive CO_2 capture as an efficient low-heat technology is thus expected to provide much lower energy consumption for regeneration with respect to rich amine solutions (*ca*. 90-160 kJ mol^{-1}).[5]

Porous solid adsorbents, such as zeolites, are potential candidates for CCUS due to their excellent working capacity and selectivity for CO_2 over other gases present in the industrial gas stream.[6] However, despite their relatively low production cost for the most common ones and high thermal/chemical stability, the detrimental competitive adsorption of water molecules significantly decreases their CO_2 working capacity and selectivity as well as requires very high temperature regeneration to desorb free water.[6b] Alternatively, amine-functionalized porous materials or porous organic materials are suitable alternative candidates.[7] For instance, Long *et al*. grafted tetraamine chains on the large pore Mg_2(dobpdc) (dobpdc = 4,4′-dioxidobiphenyl-3,3′-dicarboxylate) Metal Organic Framework (MOF) through post-synthesis modification, improving the efficiency in CO_2 capture under harsh conditions relevant to natural gas flue emissions.[8] Most notably, the relatively higher thermal stability of the tetraamine-functionalized framework was exploited, enabling a regeneration through a direct contact with steam, resulting in a significant energy saving over the conventional methods. Still, the relatively high energy penalty for the regeneration, long term stability issues, lack of sustainability and/or challenges in the up-scaling raise important limitations for the use of these classes of solids for real industrial separation processes.[9] Robust MOFs, built either from high valence metal oxoclusters/chains and poly-

carboxylates or phosphonates, or alternatively metal(II) poly-azolates, are also candidates for CO_2 capture. Their high customizability enabling a precise tuning and functionalization of the pore structure, has been intensively investigated for selective gas separation applications.[10] Indeed, one can either for instance tune their hydrophobic character to mitigate the negative effect of water, and/or modify them with exogenous chemical species for enhanced performances. Recently, CALF-20, a microporous robust Zn_2(1,2,4-triazolate)$_2$(oxalate) material (CALF stands for Calgary Frameworks) has emerged as an alternative benchmark CO_2 sorbent to standard zeolite 13X with physisorptive mechanism for the CO_2 capture from cement flue gas or high CO_2 concentration in industrial flue gases.[11] Due to its relatively moderate isosteric enthalpy of adsorption (*ca*. 40 kJ mol^{-1}), excellent CO_2 capacity in post-combustion conditions (2.47 mmol g^{-1} at 0.1 bar and 298 K), good CO_2/N_2 selectivity (230 for a $10CO_2$:$90N_2$ mixture), moderate hydrophilicity and long-term stability under real conditions, it was exploited, once coated on a rotary bed, for the capture of CO_2 in presence of moisture up to *ca*. 25-30% RH (when structured with polysulfone-based binder). This MOF was also proven to be scalable at the ton-scale using an ambient pressure optimized protocol leading to an estimated production cost of *ca*. 25-30 $/kg. Its production at the hundred tons scale is now on the way prior to being integrated into larger scale flue gas capture units in cement industry. Fluorinated MOFs, such as SIFSIX- and TIFSIX-based MOFs or NbOFFIVE-1-Ni, are also considered as potential candidates for post combustion capture due to their outstanding CO_2 adsorption capacity and CO_2/N_2 selectivity.[12] However, their long-term hydrolytic stability is in most cases limited, while their large-scale production is still hampered with strong safety (and cost) issues, mainly due to the potential formation of HF. From the material cost point of view, aluminum-based MOFs (Al-MOFs), particularly if relying on widely available low-cost commercial polycarboxylic acids, and inexpensive Al metal sources, whenever they can endow comparable CO_2 adsorption performance with CALF-20, stand as very promising candidates for CO_2 capture. One could highlight additional potential robust MOF candidates, such as A520 or Al fumarate,[13] MOF-303,[14] MIL-160(Al),[15] (MIL stand for Materials from Institute Lavoisier) which can be obtained at multi-kg scale via facile, green and one-pot synthesis procedure and simply manufactured as structured adsorbents, *e.g*., pellets, beads, monoliths and fibres. However, their CO_2 capacity is usually significantly lower compared to the benchmark

CALF-20.

In this regard, we selected the robust microporous aluminum 1,2,4,5-benzene tetracarboxylate framework MIL-120(Al), due to its excellent CO_2 capture efficiency at relatively low pressure (1.9 mmol g^{-1} at 0.1 bar at 298 K), comparable to the best amine-free benchmark CO_2 adsorbents, as well as its potentially cheap production cost. Indeed, the high affinity of this MOF for CO_2 was initially (briefly) described by Loiseau *et al*. more than a decade ago.[16] Thus, due to its promising performances, we have further explored this MOF through an in-depth joint experimental/computational study to shed light on the key features driving its remarkable CO_2 adsorption performances. Monte Carlo simulations, confirmed by *in situ* IR spectroscopy, *in situ* PXRD and low-pressure adsorption experiments, showed that the high density of μ_2-OH groups as well as the accessible aromatic rings decorating the channels play a pivotal role on the CO_2 adsorption at very low pressure, with a relatively moderate isosteric enthalpy of adsorption (Q_{st}) (~40 kJ mol^{-1}) (comparable to benchmark CO_2 physisorbents). This MOF also possesses high CO_2/N_2 selectivity (> 100) for binary gas mixtures $15CO_2$:$85N_2$ and $5CO_2$:$95N_2$ at 298 K and 1 bar, as estimated based on the Ideal Adsorbed Solution Theory (IAST), further confirmed by real coadsorption experiments. Indeed, all these features confer MIL-120(Al) a high potential for CO_2 capture from flue gases. An *in situ* synchrotron radiation Powder X-Ray Diffraction (SRPD) experiment was also carried out to better understand the structural behavior of these microporous frameworks and revealed that unlike MIL-120(Al)-HP, MIL-120(Al)-AP exhibits a phase transition, from monoclinic to triclinic, during the removal of the guest (water) molecules. Furthermore, as this material was initially made under hydrothermal conditions, an alternative eco-friendly ambient-pressure (AP) synthesis procedure was developed relying on cost-effective chemicals suitable for the easy scale-up of MIL-120(Al)-AP, while keeping an excellent crystallinity and porosity, comparable to the high pressure sample, denoted MIL-120(Al)-HP (HP stands for High Pressure). Finally, breakthrough curve measurements confirmed the efficient adsorptive separation of CO_2/N_2 using MIL-120(Al)-AP. Besides, as MIL-120 is slightly more hydrophilic than CALF-20, an advanced *operando* IR study was carried out and evidenced a faster sorption kinetics for CO_2 *versus* H_2O, suggesting the potential of MIL-120(Al) for CO_2/N_2 separation in the presence of water when an adequate fast cycling process design is applied. Finally, a techno-economic analysis was performed with the aim of assessing the production costs of this material, considering a large

production scale of 1 kton/year, that would cover less than 5% of the needs of existing cement plants worldwide and is much lower than the market scale of performant adsorbents,[17] revealing a production cost of 13 $/kg.

2. Results and discussion

2.1. Structure, synthesis optimization and adsorption performances

The crystal structure of MIL-120(Al) or $Al_4(OH)_8(C_{10}O_8H_2)$ xH_2O (x=4.8~5) was reported more than a decade ago by Loiseau *et al*., the MOF being prepared through a hydrothermal route.[18] Its inorganic sub-unit is composed of $Al(OH)_4O_2$ octahedra, with oxygen atoms from four hydroxyl groups and two different carboxylate groups belonging to two neighboring organic ligands (pyromellitate or 1,2,4,5-benzene-tetracarboxylate, abbreviated $BTeC^{4-}$). This results in infinite Al hydroxo-chains, rather uncommon in Al-MOFs, built of *trans-cis* edge sharing $Al(OH)_4O_2$ octahedra linked via double μ_2-OH bridges. These chains are linked together through the four carboxylates of the $BTeC^{4-}$ (hereafter BTeC), thereby generating a three-dimensional framework that delimits one dimensional (1D) narrow channels running along [0 0 1] direction with a free section dimension of about 5.4 Å x 4.7 Å (**Figure 1A**). Therefore, in comparison with other corner-sharing modes commonly present in most Al-MOFs (**Figure 1B**), MIL-120(Al) provides not only two-fold denser hydroxyl polar groups, which could be beneficial for enhanced CO_2 interactions with the framework, as well as four times less organic spacer per metal center, which might be highly beneficial to reduce the cost production at large scale as it is admitted that the MOF production cost is intimately correlated to that of the usually rather expensive organic ligand.[17] We also considered that this high L/M ratio as well as the four connectivity of the ligand, could lead to enhanced chemical and thermal stabilities; for instance it is well known that the Fe tetracarboxylate MIL-127(Fe) is slightly more chemically stable than the iron trimesate MIL-100(Fe).[19] Another feature that has motivated us to explore the capabilities of this MOF for CO_2 capture is the parallel arrangement of the aromatic groups of BTeC with a distance ranging between 6.5 - 7.0 Å (out of van der Waals radii) (**Figure 1C**), recently predicted by Smit *et al*. as ideal adsorbaphore for CO_2.[20]

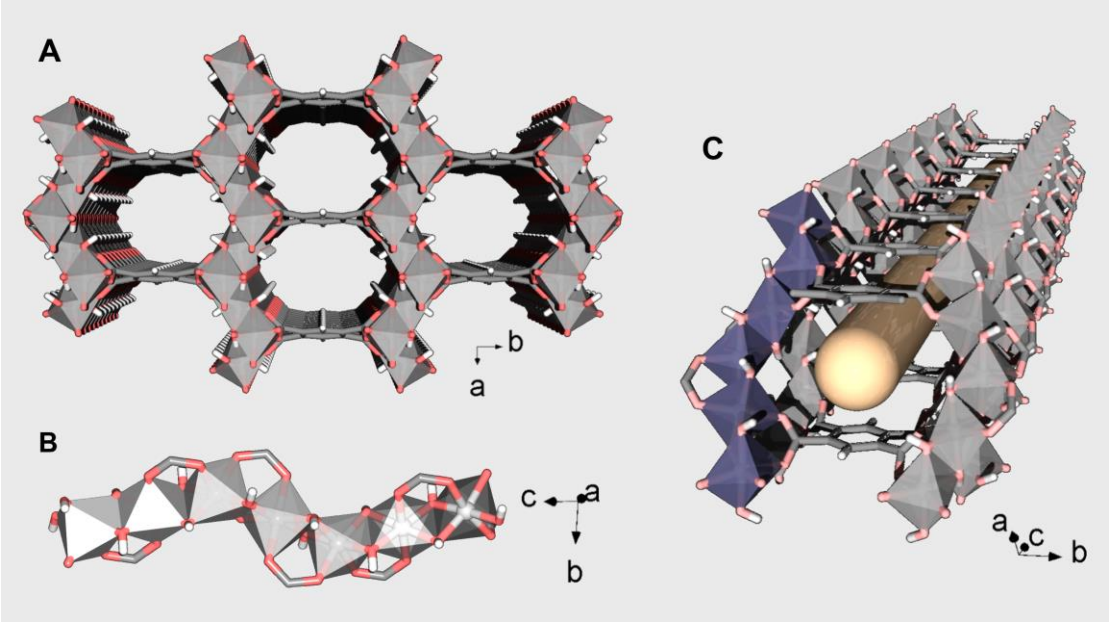

Figure 1. Crystal structure of MIL-120(Al). (A) General view along [0 0 1] highlighting the MOF narrow channels (water molecules were omitted for clarity). (B) Constitutive Al hydroxo-chains built of *trans-cis* edge sharing $Al(OH)_4O_2$ octahedra. (C) Representation of one channel emphasizing its highly confined environment (represented by the yellow tube) due to dense network of μ_2-OH and stacked phenyl rings of BTeC. Color code: $Al(OH)_4O_2$, gray polyhedra; C, gray; O, light red; H, white. In (C), one of the chains is highlighted using purple polyhedra.

The high-pressure CO_2 adsorption isotherm reported in 2009 showed already promising performances in terms of CO_2 uptake while Stylaniou *et al*., during the course of our study,[21] reported new insights over the CO_2 capture properties under post-combustion conditions with however details about the mechanism in play.[22] In both cases the authors also relied exclusively on the hydrothermal sample, limiting the chances of synthesis scalability at a reasonable cost. Herein, for the sake of understanding, we first prepared MIL-120(Al)-HP following the reported hydrothermal synthesis, and collected the CO_2 adsorption data at 298 K. Indeed, the obtained isotherm confirmed, as expected, the promising CO_2 capacity at low pressure (**Figure 2A**). Motivated by these attractive adsorption performances, it was of a crucial importance to obtain this MOF following a simpler, safer, scalable and cost-effective synthesis protocol in view of the large-scale production and further exploitation in real separation processes. Therefore, we carried out a thorough systematic experimental study to set up an optimized green synthesis at ambient pressure. Taking into account that the H_4BTeC -

Al(III) system is quite complex to optimize as different MOFs such as MIL-118(Al) and MIL-121(Al) can easily be formed once exploring this system.[23]

While both are based on more common infinite chains of *trans*-connected corner-shared aluminum-centered octahedra, similar to that of MIL-53(Al)'s, in the case of MIL-121(Al), the ligand only involves two carboxylate groups to bridge the chains, leaving the remaining two others free, pointing towards the center of the channels. If the ratio Al/H_4BTeC/H_2O has a direct influence on the crystallization of the different phases, the initial pH of the reaction mixture was shown to be of major importance. Indeed, it was demonstrated, in the previously studied hydrothermal conditions, that the occurrence of MIL-120(Al), showcasing the highest density of μ_2-OH and up to 4-fold higher Al/BTeC ratio, is driven by a basic pH > 10 (*ca*. 12 *versus ca*. 2 and 1.4 for MIL-118(Al) and MIL-121(Al), respectively). These observations were capital to optimize the synthesis conditions under ambient pressure. Thus, we selected less acidic Al-precursors to promote the formation of edge-sharing Al-chains, while we varied the Al/H_4BTeC ratio, the concentration and additives to control the pH/solubility. More details are provided in Table S1. The use of $Al(OH)_3$ systematically led to the formation of the MIL-121(Al) phase. Despite the basic nature of this precursor, its limited solubility in water resulted in acidic pH conditions attributed to the gradual dissolution of H_4BTeC occurring at a faster rate. To reach a higher solubility of the Al precursor, we first explored the $Al(OH)(OAc)_2$ (OAc stands for acetate) which has a weakly basic character and a relatively good solubility in water, while the released acetate groups can also contribute to control the crystallization process (as modulators). Interestingly, all the trials with different Al/H_4BTeC ratios (ranging from 2 to 8) yielded MIL-120(Al) phase as a sole, pure and well crystallized structure, whereas the pH at the end of the reaction was neutral. It should, however, be noted that monitoring the starting pH can be misleading because of the higher solubility of H_4BTeC compared to $Al(OH)(OAc)_2$ at room temperature (RT). These first optimizations were carried out in 15-30 mL of water leading to *ca*. 1 g product. We then opted to reproduce similar synthetic conditions at a slightly larger scale reacting stoichiometric precursors amounts (4Al/1BTeC: 80 mmol/20 mmol) in 300 mL in water to yield *ca*. 10 g of MIL-120(Al)-AP, which was further thoroughly washed in warm water whose high purity was verified by a large set of complementary characterizations including PXRD, Fourier-Transform Infrared (FT-IR) spectroscopy, Thermal-Gravimetric Analysis (TGA), N_2 adsorption at 77 K, CO_2, and water adsorption isotherms at 298 K (see supplementary

information for details, **Figure S1**).

Indeed, the PXRD pattern of the synthesized MIL-120(Al)-AP sample is in excellent agreement with the theoretical one calculated from the crystal structure (**Figure S1A**), with however a slightly broader profile compared to that of MIL-120(Al)-HP, mainly due to the difference of particle sizes (*i.e.*, few microns *versus* submicron, for the HP and AP syntheses, respectively). FT-IR spectra and TGA analyses (**Figure S1B&C**) also showed both a very good agreement for the samples obtained from hydrothermal and ambient pressure methods, although the steps of the TGA curves were slightly less well defined in the case of MIL-120(Al)-AP and a total decomposition occurring *ca*. 50 °C lower compared to MIL-120(Al)-HP. Unexpectedly, the N_2 isotherms measured at 77 K (**Figure S1D**) showed a significant difference in uptakes, with an almost 2-fold higher compared to the reported values, in favor of MIL-120(Al)-AP, with a calculated BET surface area for the latter of about 590 $m^2 g^{-1}$. This could be attributed to a potential shrinkage/flexibility of the structure at 77K more or less pronounced depending on the particle size. However, in our case, the experimental water adsorption isotherms of MIL-120(Al)-HP and MIL-120(Al)-AP at 298 K (**Figure S1E**) gave similar profiles and uptakes, noting here that the high density of μ_2-OH groups in this structure confers to MIL-120(Al) a rather hydrophilic character. Furthermore, single-component adsorption isotherms of CO_2 and N_2 were carried out at 298 K. As shown in **Figure 2A**, the CO_2 uptake in MIL-120(Al)-AP was 1.90 mmol g^{-1} (73.1 cm^3 cm^{-3}, based on the crystallographic density, 1.57 cm^3 g^{-1}, as calculated for the reported crystal structure,[18] without taking into account any guest molecule) and 3.87 mmol g^{-1} (148.8 cm^3 cm^{-3}, STP) at 0.1 and 1 bar, respectively, which is comparable, although slightly higher, to that of the hydrothermally synthesized sample and the very recent reported results reported by Stylaniou *et al*, suggesting a better activation or purity in our case.[22] Noteworthy, the occurrence of a small step at 0.35 bar of CO_2 occurs only in the case of MIL-120(Al)-HP. Additionally, under the same measurement conditions, MIL-120(Al)-AP adsorbed a much lower amount of N_2 (0.32 mmol g^{-1} at 0.9 bar). Estimation of the CO_2/N_2 selectivity was performed by applying the Ideal Adsorbed Solution Theory (IAST) model (see **Table S2**) and revealed for MIL-120(Al)-AP an excellent selectivity, higher than 100 when calculated for binary gas mixtures $15CO_2$:$85N_2$ and $5CO_2$:$95N_2$ at 298 K, 1 bar (**Figure 2B**). This confirms the high potential of MIL-120(Al)-AP for the separation of CO_2 from flue gases (5-30% CO_2) such as those emitted from industrial plants or other sources. Meanwhile, coverage-dependence of

Q_{st} was determined for CO_2 in MIL-120(Al)-AP by applying the Clausius-Clapeyron equation to single component adsorption isotherms collected at 298 K, 308 K, and 318 K (**Figure S2**). The experimental Q_{st} of CO_2 at near-zero coverage was found to be 41 kJ mol^{-1} (**Figure 2C**), close to the value reported previously for benchmark CO_2 adsorbent CALF-20 (*ca*. 40 kJ mol^{-1}). Interestingly, this Q_{st} shows only a minor decrease (about 5 kJ mol^{-1}) with the increase of CO_2 loading. The overall results strongly suggest the good CO_2 capture performance of this MOF due to its potential high CO_2 working capacity, high CO_2/N_2 selectivity, while still exhibiting a relatively low energy for regeneration. As highlighted in **Figure 2D** and **Figure S3**, it is noteworthy to mention that at 0.1 bar and 1 bar at 298 K, the CO_2 uptake of MIL-120(Al)-AP is comparable to those of benchmark CO_2 adsorbents (if not higher in some cases), such as MOF-based adsorbents (CALF-20,[11] Mg-MOF-74,[24] UTSA-16,[25] ALF (Al-Formate MOF),[26] SIFSIX-3-Cu,[27] mmen-Mg_2(dobpdc),[8] SIFSIX-3-Zn,[12c] Ni-MOF-74[28]) as well as several cationic zeolites (NaX,[29] ETS-4/10,[30] ETS stands for Engelhard Titanium Silicates).

In fact, if the performances are crucial features for a given application, other aspects including the material's cost, sustainability, chemical and thermal stability, and processability, are also important criteria to take into account, in particular when it potentially implies a very large-scale application such as CO_2 capture requiring a huge amount of adsorbents, *i.e*., more than a few hundred tons per plant.[31] TGA coupled with variable-temperature PXRD analysis (**Figure S4**), confirmed that MIL-120(Al) exhibits an excellent thermal stability (up to 400 °C), although some small variations in diffracted Bragg peaks could be observed starting from 100 °C, very likely due to a slight structural flexibility induced by guest removal and/or some bond rearrangement (*e.g*., OH groups, *etc*.). Moreover, MIL-120(Al)-AP also showed an exceptional hydrolytic stability, withstanding to boiling water for (at least) 10 days as confirmed by the well-preserved crystallinity, chemical composition, morphology, thermal stability and CO_2 capacity, as per the provided PXRD and CO_2 adsorption data, respectively (**Figure S5**). This is, to our knowledge, the most hydrothermally stable Al-carboxylate based MOF reported to date. Consequently, this encouraged us to further characterize deeply the CO_2 adsorption behavior of MIL-120(Al)-AP.

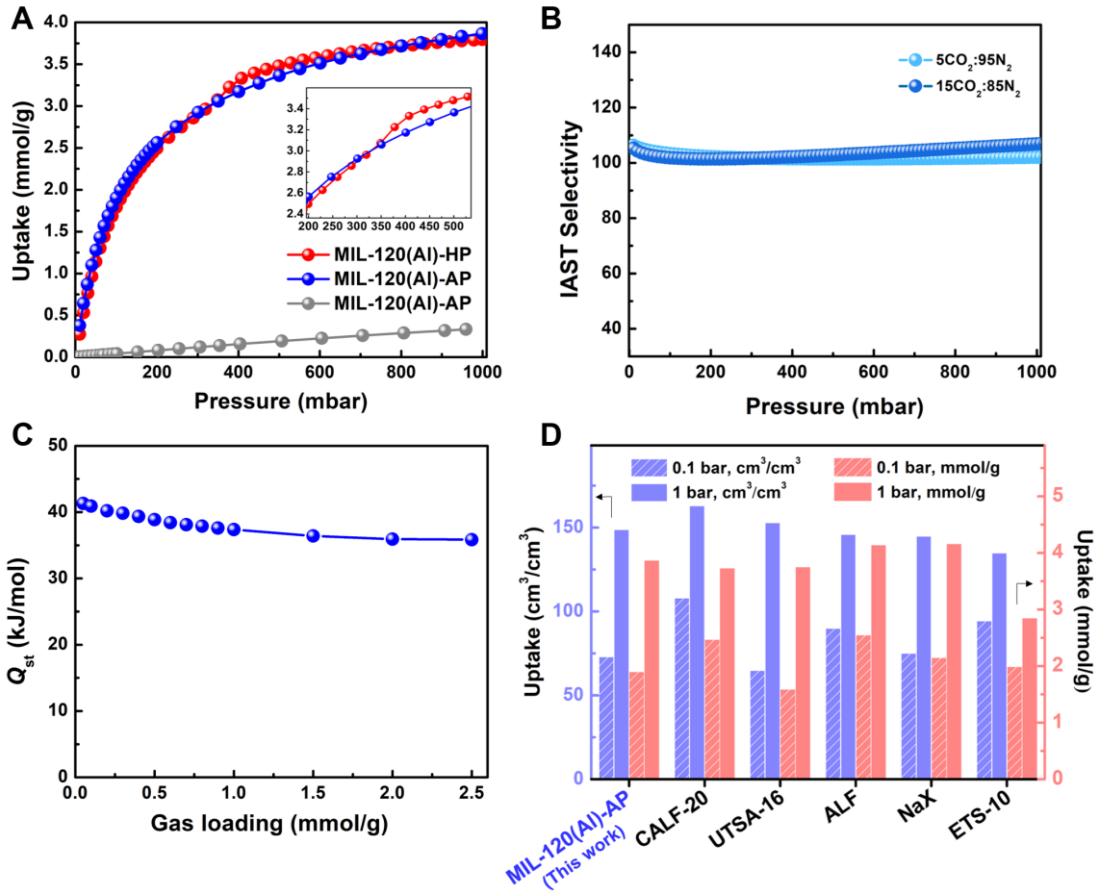

Figure 2. CO_2 adsorption performances of MIL-120(Al)-HP and MIL-120(Al)-AP at 298 K. (A) CO_2 (in red and blue, respectively) and N_2 (in gray) adsorption isotherms at 298 K. Enlargement on the step region is given in the inset. (B) IAST selectivity at different compositions for MIL-120(Al)-AP. (C) Isosteric enthalpy of adsorption *versus* CO_2 uptake for MIL-120(Al)-AP. (D) Comparison of volumetric and gravimetric CO_2 uptakes at 0.1, 1 bar, at 298 K between MIL-120(Al)-AP and benchmark adsorbents including MOFs and zeolites. The volumetric uptake was calculated using the crystallographic density.

2.2. *In situ* synchrotron radiation powder diffraction (SRPD) studies

In comparison with MIL-120(Al)-HP, the CO_2 adsorption isotherms of MIL-120(Al)-AP do not exhibit any step behavior during CO_2 adsorption, and this is regardless of the purification quality and the activation temperature. In an attempt to better understand this intriguing behavior and to shed light on the preferential interaction sites between CO_2 and the porous framework, pressure- and temperature-variable *in situ* SRPD collected at BM01 from the Swiss-Norwegian beamlines (SNBL) at the European Synchrotron Radiation Facility (ESRF, Grenoble in France) for both samples were

carried out, by monitoring the SRPD patterns starting from the activation processes (heating up to 400 K under dynamic secondary vacuum) and during all over the CO_2 loading up to 4000 mbar. Variable temperature SRPD data collected directly during activation steps are depicted in **Figure 3**.

In the case of MIL-120(Al)-HP, the analysis of the SRPD patterns evolution during the heating process revealed that the related crystal systems and space groups remained unchanged (monoclinic, *C*2/*m* (*n*°15)), despite minor variations in cell parameters, particularly an increase of the β angle and *c* parameter (**Figure 3A** and **Figure S6**). Unexpectedly, MIL-120(Al)-AP displayed a different behavior associated to a phase transition at around 350 K from monoclinic (*C*2/*m*) to triclinic (*P*-1 (*n*°2)) phase (**Figure 3B** and **Figure S11** and **S12**). The differences in particles sizes (micrometrics *versus* submicronic for HP and AP phases, respectively) could explain the difference in behavior.[32] According to the refinement of crystal structures with the Rietveld method in Fullprof,[33] for samples having been heated up to 400 K (for MIL-120(Al)-HP) or 373 K (for MIL-120(Al)-AP) and cooled to 298 K, showed in both cases, that water molecules have been removed from the pores (see **Figure S8** and **S13**). The detailed description of the SRPD is included in the Supporting Information.

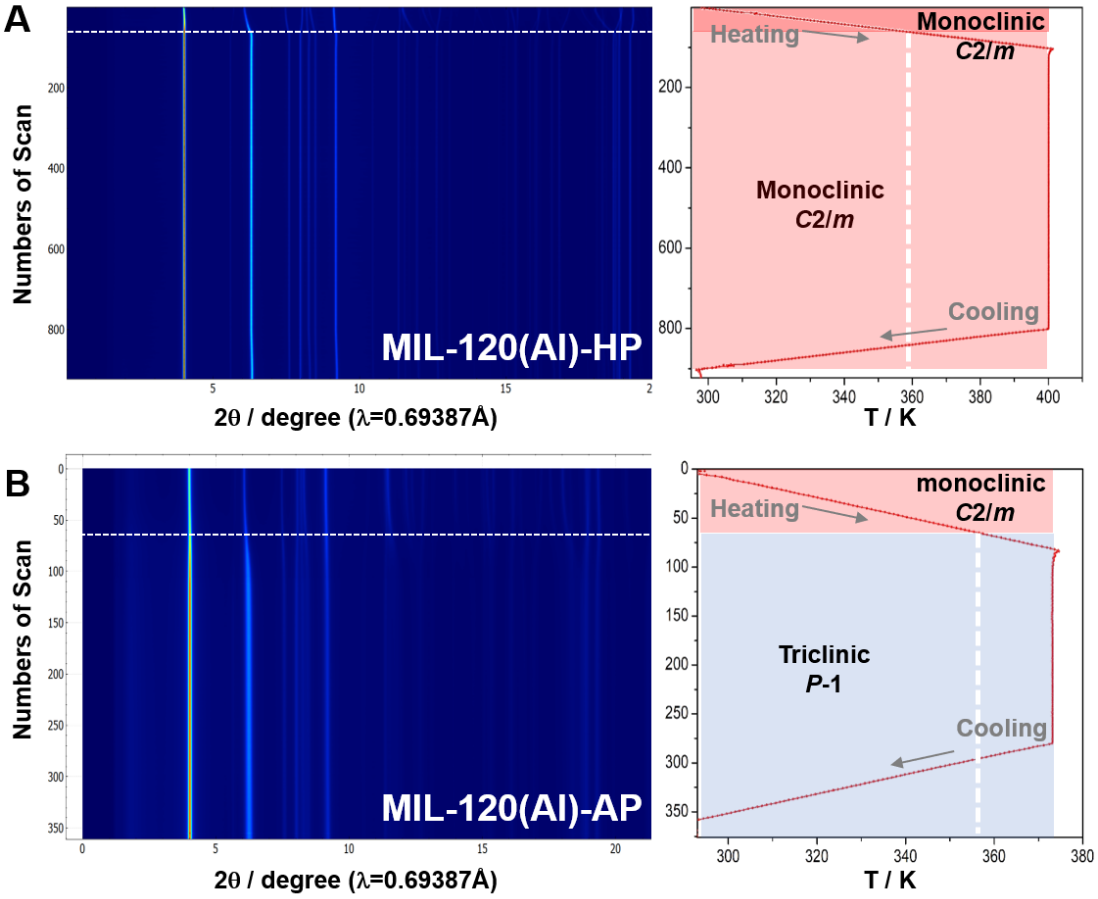

Figure 3. Variable temperature synchrotron SRPD data. Measurements performed under dynamic vacuum (activation step) for (A) MIL-120(Al)-HP, showing no phase transition, while remaining monoclinic; and (B) MIL-120(Al)-AP revealing phase transition, at *ca*. 357 K, from monoclinic to triclinic phase. Heating rate is equal to 6 K min^{-1}, up to 373 K in (A) and 400 K in (B).

The steady adsorption loadings of CO_2 at 298 and 200 K were further investigated for both samples. In particular, for a deeper understanding on the positions of CO_2 molecules and their interactions with the framework, the loading under different pressures up to 4 bar of CO_2 at 298 K was investigated for MIL-120(Al)-HP. The positions of the CO_2 molecules were found for this high pressure by the direct space methods in FOX[34] and were refined using the Rietveld method in Fullprof.[33] The MIL-120(Al)-HP sample shows a phase transition from *C*2/*m* (*n*°15) to *P*-1 (*n*°2), contrary to the MIL-120(Al)-AP, which maintains the same space group up to 1.5 bar in this study. The crystal structure refinement of MIL-120(Al)-HP suggests fully occupied CO_2 molecules located along [0 0 1] channels, showing the van der Waals O···O guest-host interatomic distances of 3.37 and 3.46 Å as well as intermolecular

O···O separations of 2.95 Å. In order to minimize the motion effects and to get higher gas loading, the emptied (dynamic vacuum) sample was cooled down to 200 K and CO_2 was loaded stepwise again up to 1 bar. The *P*-1 crystal structure remained for MIL-120(Al)-HP at these conditions. The previous CO_2 molecules kept their location along the [0 0 1] channels (with a slight shift), however one more independent molecule is expected in the middle of the pore (with ½ of occupancy), laying between their two arrays, see (**Figure 4A**). Each array is composed of alternated CO_2 molecules with occupancies of *ca*. 0.82 (**Figure 4B**). As depicted in **Figure 4C**, a closer look on the interaction of these molecules with the frameworks showed (i) that CO_2 are mainly interacting with the μ_2-OH groups (*d*(O···O) ranging from *ca*. 3.03 Å to 3.34 Å), while (ii) the second CO_2 interacts with two μ_2-OH between the opposite Al-oxo chains with relatively weaker interactions (d(O···O) ≈ 3.43 Å and 4.01 Å); and from another side with the aromatic phenyl rings that belong to two stacked BTeC (delimiting the channels) via dispersion and electrostatic interactions (very likely between the carbon of the aromatic ring and the central carbon atom of CO_2, in addition to further interactions between one electropositive aromatic H atom (not localized in this structure) and one electronegative O atom of CO_2).[35] As it was mentioned, the MIL-120(Al)-AP sample remains without any significant changes at 298 K (at least up to 1.5 bar), however at 200 K and 1 bar of CO_2, it adopts monoclinic *C*2/*m* crystal structure with the similar to MIL-120(Al)-HP two independent CO_2 molecules. The two arrays of CO_2 molecules have a similar to MIL-120(Al)-HP (*ca*. 0.82 occupancies) and are located in parallel to each other in front of two μ_2-OH (d(O···O) 3.06 Å). They have a comparable intermolecular distance of d(C···C) 3.05 Å. The second CO_2 molecule fully occupies the center of the pore and has a bit longer connectivity with four μ_2-OH (d(O···O) 3.26 Å) and shorter d(O···O) 2.60 Å intermolecular contacts with other CO_2 molecules. More details about the phase transition analysis are included into the Supporting Information (**Figure S6-S14**).

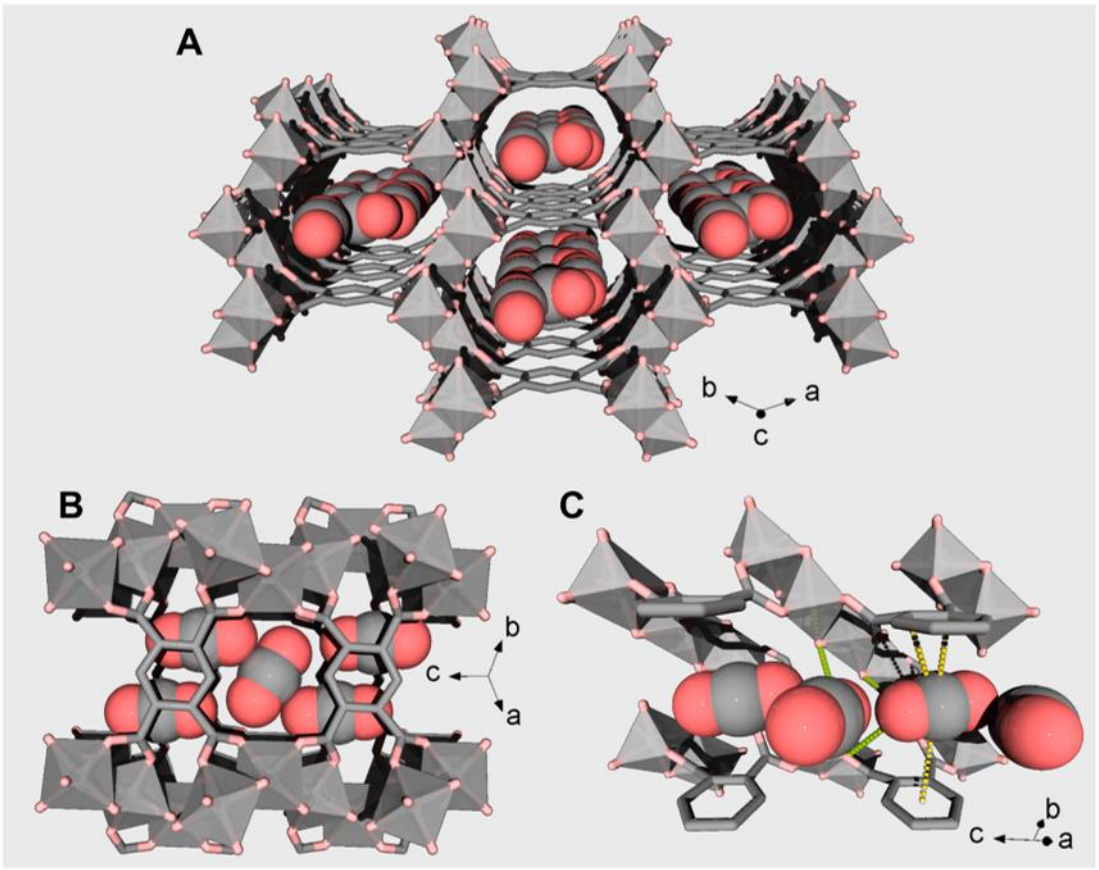

Figure 4. Crystal structure of MIL-120(Al)-HP cooled down to 200 K and loaded with 1 bar of CO_2. (A) General view along [0 0 1]. (B) Top view of a part of one channel, and (C) a cut through a channel showing the arrays of alternated CO_2 molecules and their interactions with the frameworks throughout μ_2-OH and phenyl groups of the BTeC (represented as green and yellow dashed lines, respectively). Color code: $Al(OH)_4O_2$, gray polyhedra; C, gray; O, light red. H-atoms were not localized.

2.3. Molecular simulations

The crystal structure of MIL-120(Al)-AP was first fully geometry optimized (both atomic positions and cell parameters allowed to relax) in its empty form at the Density Functional Theory (DFT) level. Since it is not possible to experimentally determine the positions of the H atoms of the framework with X-ray diffraction data, we therefore constructed a set of configurations corresponding to different μ_2-OH orientations that were subsequently geometry-optimized. Two stable structures were identified, labelled as MIL-120(Al)-AP-Str1 and MIL-120(Al)-AP-Str2 and illustrated in **Figure 5A**. The structural and textural features of these two DFT-optimized structures are in line with the experimental data collected on the MIL-120(Al)-AP sample (see **Table S3**). The X-

ray diffraction patterns calculated for these two structures showing very similar unit cell parameters/cell volume (only 2.4% cell volume difference) (see **Table S3**) are in good agreement with that collected experimentally (**Figure 5B**). The total energies of the two structures differ by 11.29 meV atom^{-1}, with MIL-120(Al)-AP-Str1 being the most stable one. Their CO_2 adsorption isotherms were further calculated at 298 K using Grand Canonical Monte Carlo (GCMC) simulations. **Figure 5C** shows that the simulated adsorption isotherm for MIL-120(Al)-AP-Str1 is in excellent agreement with the experimental data while a steeper increase of CO_2 uptake at low pressure is simulated for MIL-120(Al)-AP-Str2. This observation strongly supports that the μ_2-OH orientation plays a critical role in the CO_2 affinity of the MOF framework and indeed the most energetically stable MIL-120(Al)-AP-Str1 structure enables to capture the experimental scenario. Typically, the highly symmetric μ_2-OH orientations towards the pore channel in MIL-120(Al)-AP-Str2 induces strong direct interactions with CO_2 (see **Figure S15**) leading to a simulated adsorption enthalpy at low coverage higher compared to that calculated for MIL-120(Al)-AP-Str1 (43.8 kJ mol^{-1} *versus* 39.4 kJ mol^{-1}) in line with its steeper adsorption isotherm profile observed at low loading.

This distinct CO_2 adsorption behavior in MIL-120(Al)-AP-Str1 and MIL-120(Al)-AP-Str2 is illustrated in **Figure 5D** which reports the DFT-optimized structures for two different CO_2 loadings. We observed that at the loading of one CO_2 per unit-cell (corresponds to 2.02 mol g^{-1} CO_2 loading), CO_2 orientated parallel to the organic linker adopts a highly ordered geometry interacting simultaneously with the four μ_2-OH groups of MIL-120(Al)-AP-Str2 while for MIL-120(Al)-AP-Str1, CO_2 preferentially interacts with only two μ_2-OH groups ($d_{O_{CO_2}-O_{\mu 2-OH}}$ = 3.28 Å). This distinct adsorption behavior is in line with a higher CO_2 affinity for MIL-120(Al)-AP-Str2 and hence its resulting steeper adsorption isotherm at the initial stage of adsorption. When CO_2 concentration increases up to two molecules per unit-cell (corresponds to 4.05 mol g^{-1} CO_2 loading), **Figure 5D** also reveals a similar simulated guest distribution in both MIL-120(Al)-AP structure models with associated $d_{O_{CO_2}-O_{\mu 2-OH}}$ distances of 3.30 Å and from 3.08 to 3.17 Å for MIL-120(Al)-AP-Str1 and MIL-120(Al)-AP-Str2, that match well with the experimental reported data shown in **Figure 4A** and **4B**.

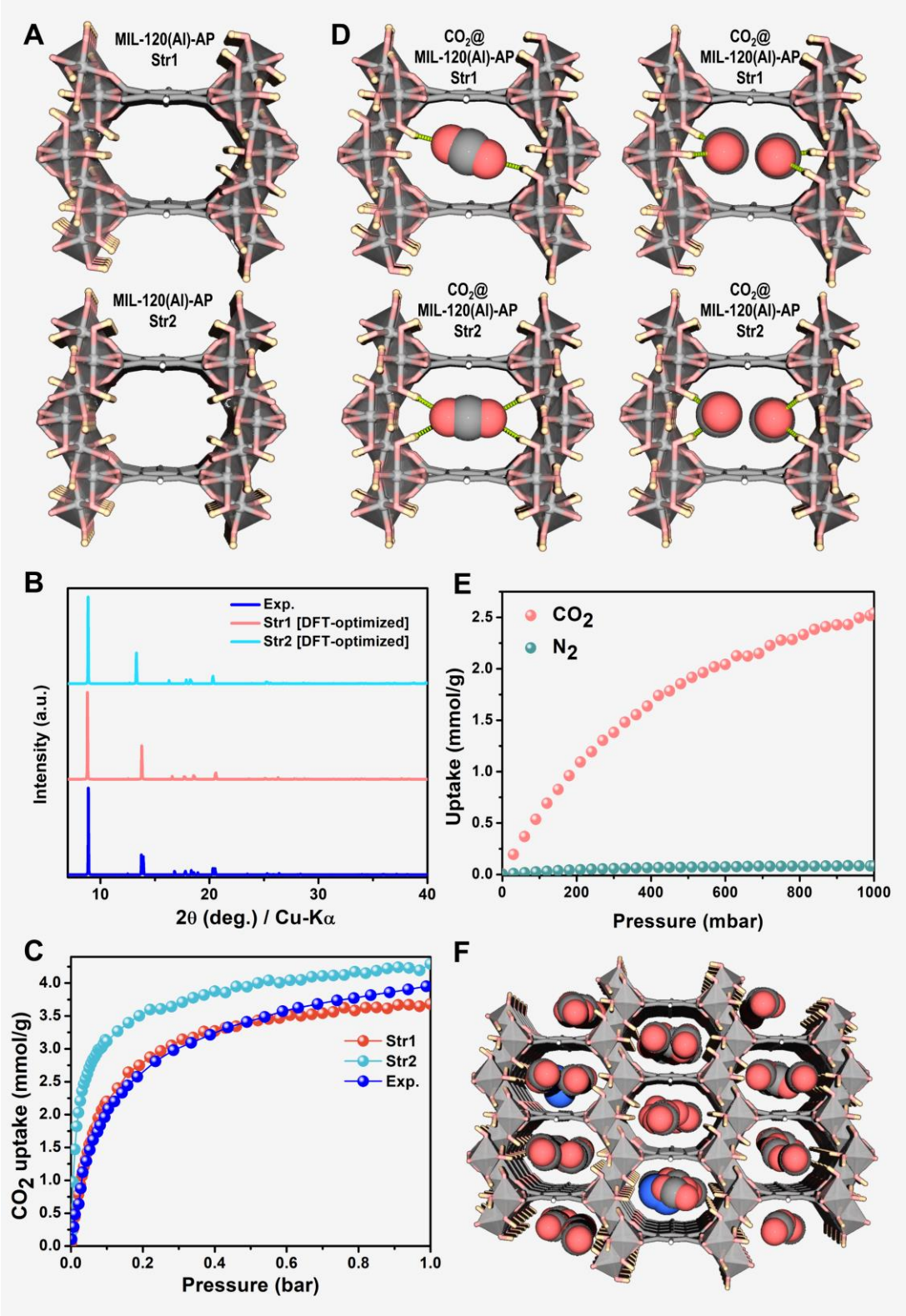

Figure 5. Molecular simulations of MIL-120(Al)-AP structure and adsorption properties. (A) Most stable DFT-optimized structure of MIL-120(Al). The unit cell parameter is not shown to highlight the different orientations of μ_2-OH group in the channel. The most stable Str1 and Str2 structures correspond to distinct orientations of

μ_2-OH groups [details in Supporting Information]. (B) Calculated X-ray diffraction patterns for the two most stable DFT-optimized MIL-120(Al)-APs and the corresponding experimental data. (C) GCMC-simulated and experimental single-component CO_2 adsorption isotherms at 298 K. (D) Illustrations of the DFT-optimized CO_2-loaded MIL-120(Al)-AP-Str1 and MIL-120(Al)-AP-Str2 structures with different CO_2 loading (one [top] and two [bottom] CO_2 molecules per unit-cell). The dashed line represents the interaction between the CO_2 molecule (O) and the μ_2-OH group (H) of the framework correspondingly. (E) GCMC-simulated $15CO_2$:$85N_2$ binary mixture adsorption isotherm of MIL-120(Al)-AP-Str1 at 298 K calculated by GCMC simulations, (F) Corresponding snapshot (zoom in) showing the location of CO_2/N_2 in MIL-120(Al)-AP-Str1 at 1 bar and 298 K from GCMC simulation (*cf*. full sharpshot in **Figure S16**). Color code in A, D and F: $Al(OH)_4O_2$, gray polyhedra; C, gray; O, light red; H, white (C-H) and light yellow (O-H); N, blue. Interactions between CO_2 molecules and μ_2-OH groups are represented as green dashed lines. All views are shown along [0 1 1].

Next, the $15CO_2$:$85N_2$ binary mixture adsorption isotherm was simulated for MIL-120(Al)-AP-Str1 (**Figure 5E**). This structure model is predicted to predominantly adsorb CO_2, while N_2 uptake is almost negligible over the whole pressure range up to 1 bar. **Figure 5F** evidences that CO_2 molecules are mostly located at the same positions than in single components while only a very few N_2 molecules are adsorbed in the MOF pores. The resulting CO_2/N_2 selectivity is comprised between 110~170 (see **Figure S17**), which is in good agreement with the IAST estimations obtained from the experimental single component adsorption isotherms, further confirming the great potential of MIL-120(Al)-AP for CO_2 capture from flue gases.

2.4. Green scalable synthesis

As mentioned earlier, MIL-120(Al)-AP possesses a high ratio of metal to ligand (4:1), which is (by far) higher than for the other MOFs. Since the ligand is the main limiting component in MOFs' production cost, particularly when abundant metal cations are in play,[17] this shall be highly advantageous for a large-scale industrial synthesis. To meet with a potential use for industrial separation processes where the sorbents need to be produced at a very large scale, first attempts of kilogram-scale synthesis of the MIL-120(Al)-AP solids were carried out (synthesis methods given in Supporting Information)

based on the optimized AP synthesis method developed in this work. Considering the cost of aluminum precursors (See **Table S7**) ($Al_2(SO_4)_3$ $18H_2O$, $Al(NO_3)_3$ $9H_2O$, $AlCl_3$ $6H_2O$) and/or their low solubility, safety or corrosive issues, in addition their less acidic chemical nature (as discussed in the previous sections), two other precursors were also considered for the synthesis at larger scale (> 100 g). First, the optimized procedure using $Al(OH)(CH_3COO)_2$ was deployed, relying on a 30 L glass line reactor equipped with a pressurized filtration system (**Figure S19**), leading to a batch of MIL-120(Al)-AP up to 1-2 kg (per single synthesis). Later, a more cost-effective Al-precursor, namely $NaAlO_2$, among the less expensive Al sources, was explored and served to demonstrate the feasibility of a multi-kilogram-scale cheaper synthesis with a higher Space-Time Yield (STY).[36] In both cases, high quality MIL-120(Al)-AP materials were easily synthesized with a high yield (> 70%) at > 3 kg scales via green methods, as confirmed by SRPD patterns, FT-IR spectroscopy, TGA, N_2 adsorption (**Figure S20**), CO_2 adsorption (**Figure 6A**), and SEM/EDX results (**Figure S21** and **S22**). Noteworthy, the kilogram-scale and the small-scale samples exhibited almost the same CO_2 uptake under the same conditions. When using $Al(OH)(CH_3COO)_2$ as an aluminum precursor, water was the only solvent in the synthesis procedure, and after washing with warm water, the STY reached a moderate value close to 60 kg m^{-3} day^{-1}. When using $NaAlO_2$ as an aluminum precursor, it was necessary to add acetic acid as a pH modulator to obtain MIL-120(Al)-AP because of the too high alkaline character of the starting $NaAlO_2/H_2O$ solution. The STY value was higher, around 100 kg m^{-3} day^{-1}, due to a too higher concentration used for the reaction, which is comparable to the values obtained for zeolites (50 to 150 kg m^{-3} day^{-1}) or benchmark Al-MOFs such as MIL-160[37] or MOF-303.[14] Meanwhile, it is interesting to note the smaller particles sizes of MIL-120(Al)-AP obtained when $NaAlO_2$ is used instead of $Al(OH)(CH_3COO)_2$ as observed from SEM images (*ca*. 50 nm *versus ca*. 300 nm in large scale syntheses; **Figure S21**). This could be ascribed to a faster reaction/nucleation between Al(III) and BTeC in the case of former due to the more basic conditions favoring Al hydroxide condensation. Moreover, to assess the atomic-scale quality of the scaled-up samples, solid state multinuclear (^1H, ^{13}C, and ^{27}Al) NMR (ssNMR) Magic Angle Spinning (MAS) studies were carried out. The ^1H spectra and its decomposition in three components (**Figure S23** and **Table S8**) show that neither the synthetic route nor the scale affects significantly the proton structural environments. The ^{13}C experiments confirm this analysis: the four spectra are close-to-identical and match the literature

data. It therefore confirms that the linker local structure and arrangement is the same for all synthesis conditions and that no significant amount of organic impurities can be detected. There is only a small, but significant, increase in linewidth for the aromatic protons and the μ_2-OH for the large scale synthesis done with $Al(OH)(CH_3COO)_2$, showing a compound slightly more disordered than the other three. The ^{27}Al ssNMR MAS spectra (**Figure S24**) of the four compounds confirm this analysis: the two crystallographic sites are well identified (see MQMAS in **Figure S24**), with all NMR parameters identical within uncertainty (See **Table S9**). The exception is found again for the $Al(OH)(CH_3COO)_2$ large-scale synthesis which displays a smoothening of the line shapes, a clear indication of the presence of structural disorder, likely to be due to the higher proportion of defects generated by the residual acetates still embedded within the framework, eventually replacing some BTeC moieties. For the latter, a slightly modified chain arrangement is to be expected based on the reduction in nuclear quadrupole coupling constant C_Q (8.6 MHz to 7.7 MHz) and quadrupolar asymmetry parameter (0.5 to 0.6) of one of the aluminum sites. Finally, a shoulder at the left side of the peaks observed for the $NaAlO_2$ large scale synthesis is more intense than the "n=0" spinning sideband of the <-3/2,3/2> transition, and points to the possible presence of an oxide impurity which accounts for approx. $6\%_{at}$ of the total aluminum content (although not affecting the adsorption performances).

Considering the requirements of the real application, MOF powders need to be shaped not only to (i) avoid the tedious (and possibly risky) manipulation of powder, but also (ii) to minimize the pressure drop and thermal gradient across the adsorption column and ensure an optimal fluid and heat diffusion. Here, we have successfully shaped MIL-120(Al)-AP using inorganic binders, namely bentonite and silica, through an extrusion/spheronization method. The CO_2 uptakes of the MIL-120(Al)-AP beads obtained with 10% of silica and 10% of bentonite were in good agreement with the uptake of the MOF in the powder form (**Figure 6B**). Additionally, the MIL-120(Al)-AP beads exhibited a high and useful crushing strength particularly when using bentonite (~38 N for MIL-120(Al)-AP with 10% bentonite; ~ 9 N for MIL-120(Al)-AP with 10% silica) (**Figure S25** and **S26**) which is important for column-filling robustness during CO_2 capture applications. The higher mechanical strength of beads obtained with the aluminum silicate bentonite might be due to the strong affinity between Al-OH groups that are likely to decorate the external surface of bentonite and MIL-120(Al)-AP.

2.5. Cyclability, Breakthrough curve tests

The reusability of MIL-120(Al)-AP solids was first investigated upon six consecutive CO_2 adsorption/desorption cycles (See **Table S6**), using different temperatures for the activation. The CO_2 uptake of MIL-120(Al)-AP solids after activating the sample at 298 K under secondary vacuum during six hours in the first two measurements exhibited slightly higher values compared with the same sample after activation at 323 K, as depicted in **Figure S18**. This could be due to a slight reorganization of the μ_2-OH groups, resulting in slightly different CO_2 uptakes. After a first activation at 323 K, the CO_2 uptake did however not change much depending on the activation condition, strongly indicating that MIL-120(Al)-AP keeps a reproducible CO_2 uptake due to the dense μ_2-OH groups in the channels.

Finally, to study the separation performance for $15CO_2$:$85N_2$, first, dynamic column breakthrough experiments were performed using a few grams scaled-up shaped sample, in a packed column filled with activated MIL-120(Al)-AP with 10% silica and MIL-120(Al)-AP with 10% bentonite with a total flow of 1 NL min^{-1} (experimental set-up is detailed in **Figure S27**). As depicted in **Figure 6C &D** (run 1), in both cases, highly efficient separation of CO_2 from the CO_2/N_2 mixture could be achieved: N_2 gas first eluted through the adsorption bed at the beginning of the adsorption process while CO_2 appears at the outlet of the column from breakthrough time leading to a CO_2 pure productivity (0.67 mmol cm^{-3} for MIL-120(Al)-AP with 10% silica; 0.79 mmol cm^{-3} for MIL-120(Al)-AP with 10% bentonite). The breakthrough curves were used to experimentally determine the CO_2/N_2 selectivities which are as high as 93 for MIL-120(Al)-AP with 10% silica and 98-108 for MIL-120(Al)-AP with 10% bentonite, respectively, in excellent agreement with IAST calculated values on the single component adsorption isotherms collected on pure powder form. Additionally, CO_2/N_2 adsorption/desorption cycles have been carried out to evaluate the regeneration of both shaped MIL-120(Al)-AP under dry and humid conditions (experimental procedure detailed in Supporting Information). In dry conditions, a complete regeneration was observed (**Figure S28 A&B**) after four cycles without heating or vacuum conditions. However, the same measurements in humid conditions (**Figure S28 C&D**) highlighted the progressive accumulation of water between each cycle leading to a CO_2 capacity decrease in the operating conditions (*i.e.*, without heat or vacuum). After this exposure to moisture, both samples were however fully reactivated at 50 °C under vacuum. The

same breakthrough results (Run 2 in **Figure 6C&D**) were observed, strongly indicating that this MOF can provide a good repeatability of CO_2 adsorption with full regeneration after exposure to humid atmosphere, although a slight modification of the breakthrough curves could be observed in the case of beads shaped with silica. Since the regeneration was achieved by heating and vacuum, MIL-120(Al)-AP appears as a suitable adsorbent well adapted to TSA (thermal swing adsorption) carbon capture under real conditions, but also to V/PSA (vacuum swing adsorption or pressure swing adsorption) conditions when specific considerations are taken into account (*i.e.*, either pre-drying, or very fast cycling process).

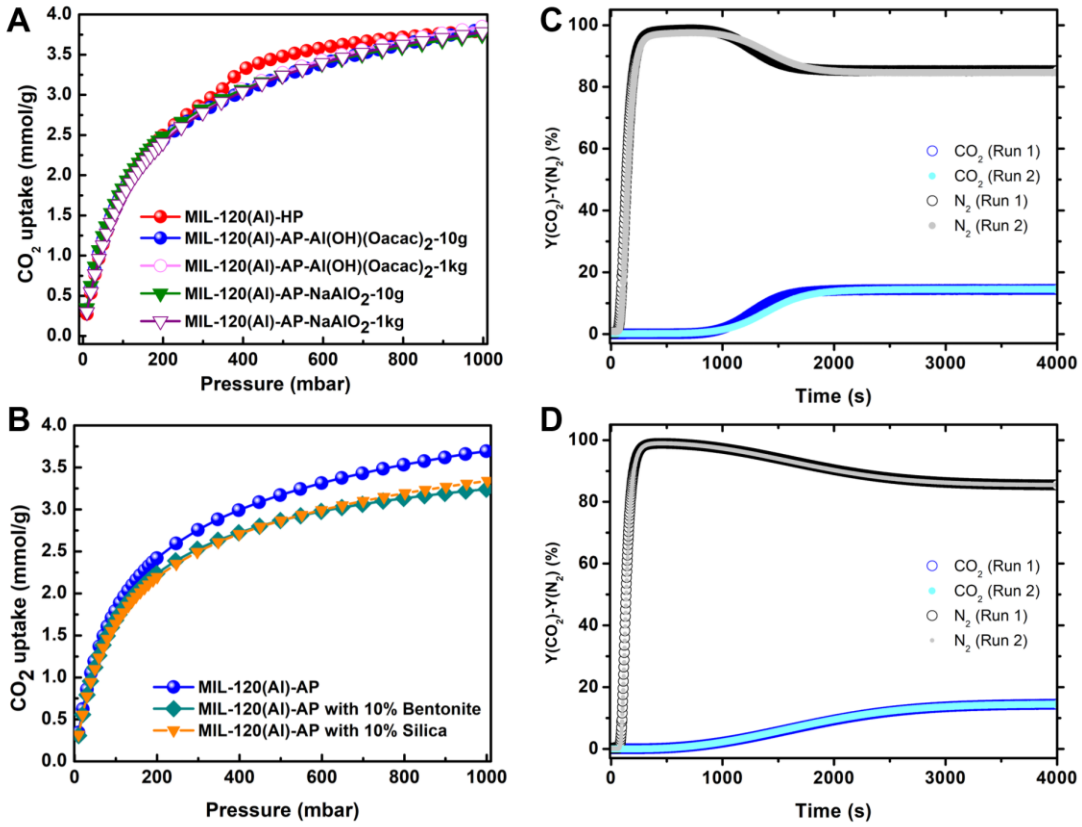

Figure 6. CO_2 adsorption uptakes of MIL-120(Al)-AP. (A) CO_2 adsorption isotherms at 298 K on different scale batch preparations. (B) CO_2 adsorption isotherms comparison between pure and structured samples with 10% Bentonite or Silica. (C) Breakthrough curves for MIL-120(Al)-AP beads with 10% Si. (D) Breakthrough results of MIL-120(Al)-AP beads with 10% bentonite. The activation condition for both samples was heating at 50 °C for 12 hours under vacuum, run 1 refers to the measurement in dry conditions, run 2 refers to the measurement in dry conditions after exposure to humid conditions, while in between the sample was reactivated at 50 °C under vacuum.

2.6. *Operando* spectroscopic studies

In order to further evaluate the potential of MIL-120(Al) for CO_2 capture at industrial scale, including in the presence of water, and for the regeneration of the MOF, *operando* infrared (IR) investigations were carried out on the MOF powder in relevant conditions, both as a self-sustained wafer and deposited on a Si plate (to monitor structural bands), in order to simulate the material behavior at duty. Therefore, the sample was first subjected to an activation step by flowing pure Ar at RT followed by a heating ramp (in Ar) after a steady state was achieved at RT. The desorption of any species, paying particular attention to water molecules, was monitored by Mass Spectrometry (MS) and IR. A first rapid water release was observed, finishing completely after eight hours at RT in Ar flow, as shown in **Figure S29**. After the steady state was achieved at RT, the sample was monitored at increasing temperatures (100-300 °C) under the Ar flow. Further water was released in the range 100-300 °C (**Figure S30**). However, residual free acid, if any, could be removed at 200 °C and structural changes are detected from 300 °C. In addition to activation at RT, a faster removal of water (in less than one hour) was evidenced when the activation was carried out in Ar flow at 100 °C. This suggests that MIL-120(Al) can be activated under mild conditions. Nevertheless, the high density of μ_2-OH groups in MIL-120(Al) leads to a highly hydrophilic character (consistent with the experimental water adsorption isotherms (**Figure S1E**)). Thus, we aimed to deeply investigate the effect of water during CO_2 adsorption after activation. *Operando* IR spectra were collected at room temperature during the adsorption of CO_2 in MIL-120(Al)-AP in the presence of 1% H_2O (a maximum concentration which could be envisaged in a CO_2 capture process after a chiller) and compared to the same conditions but in dry CO_2/Ar flow. **Figure 7** shows the *operando* IR spectra recorded *versus* time during wet CO_2 adsorption. At the beginning of the adsorption process (during *ca*. 2 min), a very fast CO_2 adsorption is observed, as witnessed by the characteristic band at 2338 cm^{-1}; meanwhile no H_2O adsorption occurs (the IR band around 3500 cm^{-1} associated to stretching vibrations of OH-bonds remains constant and the characteristic combination band associated to H_2O at 5170 cm^{-1} is still absent). Then, after about 7 min, the bands of CO_2 progressively decrease concomitantly to the slow increase of H-bonds absorbance, revealing that initially CO_2 successfully competes with water on the adsorption sites. However, after 10 min, a drastic drop of the band of CO_2 and a stable band intensity for the H_2O groups are observed, indicating that the

adsorbed CO_2 molecules have been partially replaced by H_2O molecules. This phenomenon is also observed in the MS signal, confirming that MIL-120(Al) exhibits much faster adsorption kinetics for CO_2 than for water molecules, before reaching an equilibrium favorable to water. To further clarify the rapid CO_2 adsorption in the presence of water, CO_2 adsorption was analyzed in dry or wet Ar flow at different CO_2 concentrations. As represented in **Figure S31**, the presence of H_2O does not decrease the CO_2 uptake compared with the dry conditions (considering the maximal adsorption before any CO_2 removal by H_2O in long-time term). On the contrary, small amounts of water in the flow seems to even promote the CO_2 uptake. Furthermore, the uptake of H_2O decreases slowly with increasing CO_2 concentration in the Ar flow, demonstrating that CO_2 can suppress water adsorption to a certain extent favored by kinetics. **Figure S32** (MS) and **Figures S33-34** (IR) report the quantified amount of CO_2 and H_2O adsorbed in the material. It is important to note, first, that *in situ* IR spectra of the activated sample (**Figure S34**) showed four distinct and sharp ν(O-H) stretching bands revealing four OH groups with relatively different environment in the structure, which is the first time observed in a MOF, to the best of our knowledge. These OH groups appear insensitive to activation under vacuum up to 150 °C. Furthermore, we observe that the amount of CO_2 adsorbed in the MIL-120(Al)-AP framework is proportional to CO_2 partial pressure in the flow. For instance, the intensity of CO_2 under 30% CO_2 concentration in the gas flow exhibits the highest absorbance in IR spectra. Combining these results with those from the MS signal, we can confirm that the presence of H_2O does not decrease the CO_2 uptake at the beginning of the adsorption process. Additionally, the spectra of the hydroxyls, with time on stream in a flow containing CO_2, shows that these groups are only slightly perturbed by the introduction of small aliquots of CO_2 and water in the cell and confirms the model represented in **Figure 5**, showing experimentally the interaction of the CO_2 molecules with four OH groups, inducing a progressive decrease in the pristine peaks (activated sample) and the formation of H-bonding broad bands proportionally to the CO_2 partial pressure (**Figure S34**). After one hour, however, the CO_2 uptake significantly decreases, showing that H_2O saturates the material during time on stream, significantly removing most of the adsorbed CO_2.

Therefore, these *operando* IR studies confirm the potential of MIL-120(Al) for the CO_2/N_2 kinetic separation even in the presence of water (to some extent), despite the

hydrophilic behavior revealed by the water isotherms and the preliminary results showed by dynamic breakthrough measurements operated at flowrate setpoint of 1 NL h^{-1}. This would call, however, for a specific process design taking into account the difference in adsorption kinetics between CO_2 and H_2O as well as a regeneration of the sorbent, particularly water, as it is typically done in V/PSA processes. In this regard, suitable dynamic breakthrough measurements with careful tuning of the stream flow rate and dimension of the column should be carried out for optimal process design.

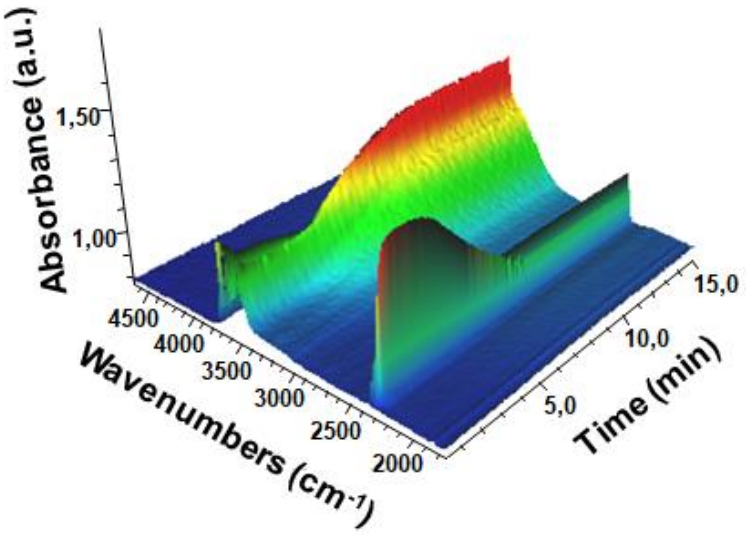

Figure 7. *Operando* IR spectra. IR spectra in the ν(OH) and ν(C=O) region for MIL-120(Al)-AP with time on stream during the first minutes of CO_2 adsorption in the presence of water (20% CO_2 and 1% H_2O in Ar flow at RT).

2.7. Techno-economic analysis for MIL-120(Al)-AP production

Based on the synthesis at pilot lab-scale (15 L scale), we propose herein an industrial-scale production process. A batch process design was considered based on process synthesis heuristics, considering a reactor STY of 100 kg m^{-3} day^{-1}. The flowsheet with the main block diagrams of the process is shown in **Figure S35**. The process rationale followed the same methodology that was previously described by some of us where the raw materials are being fed to a batch stirred reactor, the resulting solid is retrieved by filtration, followed by washing, drying and storage.[17] All the equipment was designed for a yearly production of 1 kton (the rationale behind this value was presented at the Introduction), which would represent *ca*. only 5 % of the total amount of adsorbent required to capture CO_2 on a yearly basis for the world cement industry's plants. From

the equipment size, an investment in base equipment of 2.4 M$ (2022 prices) was estimated. Using common chemical engineering process cost factor estimation methods, we calculated a total investment of 13.9 M$ (2022 prices), as detailed in **Table S10** and S11. This investment already includes the capital costs for a 60% investment loan and a project time span of 12 years (2 years for construction and 10 years of operation for amortization; more details in Supporting Information).

The production cost of MIL-120(Al) was estimated based on the manufacturing costs (direct, indirect, and fixed), and general expenses, as explained in detail in **Table S12**. The final calculated production cost is 12.94 $/kg (2022 prices), which is significantly lower than previous estimates, based on raw materials costs obtained from laboratory chemical reagents catalogs (2916.5 $/kg).[22] Comparing with previous estimates for MIL-160(Al) made by some of us in 2019 (29.5 $/kg for 1 kton/year),[17] the MIL-120(Al) production cost scaled to 2019 prices is significantly lower (9.86 $/kg). This is due to two cumulative factors related with the ligand that are favorable for MIL-120(Al): the lower ligand-to-aluminum mass ratio and the lower price of the ligand. The BTeC ligand in MIL-120(Al) is (at least) ten times less expensive than the 2,5-furandicarboxylic acid ligand in MIL-160(Al). Some of us have also recently estimated a production cost for MIL-100(Fe) of 30 $/kg for a 1 kton/year production,[38] which is also higher than that for MIL-120(Al).

To better understand how the estimated production cost could vary, we performed a sensitivity analysis to our economic model. From the structure of the direct production costs (See **Table S12**), one can observe that the main contribution arises from the raw materials (*ca*. 45%). From these, the ligand price is the most significant and prone to variations (sodium aluminate and acetic acid are common raw materials used in the industry). Thus, we selected the ligand price as one of the variables for the sensitivity analysis. Since the price of electricity has increased significantly over the last three years,[39] we have selected this factor as another variable for the sensitivity analysis. We can observe that the ligand price has a stronger influence on the production cost, with a variation from 12.33 to 23.92 $/kg when the price of the ligand varies between 0.5 and 10 $/kg (**Figure 8A**). The energy cost has a lower impact on the production cost, with a variation of 12.13 to 13.52 $/kg, considering a span of energy prices from 0.032 to 0.242 $/kWh. Since investment estimates based in historical equipment prices are always approximations, and the chemical engineering equipment cost has been increasing significantly in recent years,[40] we have also looked at the influence of the

base equipment cost on the production cost (**Figure 8B**). A variation of ± 1.11 $/kg is observed when the base equipment cost varies by ± 20%. Thus, the production cost of MIL-120(Al) seems to be more influenced by the ligand price but, nevertheless, it remains significantly lower than other previous estimations for this and other MOFs. For larger production scales, this cost is expected to be even lower due to the principle of the economy of scale. Moreover, with a prospect of some further improvements in the synthesis procedure, we could, for instance, by shortening the synthesis duration to 13 h, significantly increase the STY = 190 kg m^{-3} day^{-1}) without hampering the product quality and CO_2 performance (**Figure S36**). Therefore, this will bring the estimation cost to even more attractive values and lead to a higher production per year.

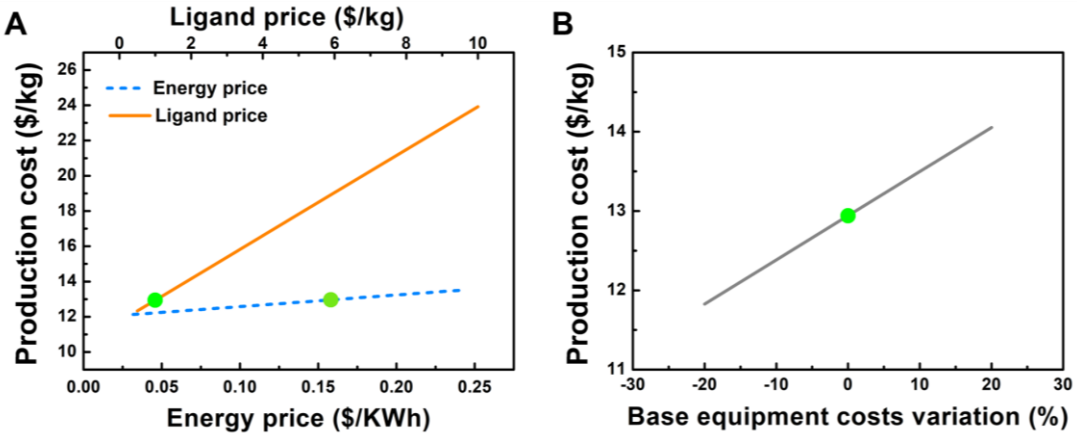

Figure 8. Sensitivity analysis of MIL-120(Al)-AP production costs. (A) Effect of the ligand and energy costs; (B) effect of the base equipment costs. The green dots over the lines represent the base economic scenario (2022 prices).

3. Conclusion

In this work, a highly robust and cost-effective aluminum-based microporous Al tetracarboxylate MOF, MIL-120(Al), was thoroughly studied in a view of post-combustion carbon capture applications. An environmentally friendly and economically viable ambient pressure synthesis route was developed leading to pure MIL-120(Al)-AP samples, as an alternative to the previously high temperature hydrothermal route. A combination of experimental and computational adsorption results first confirmed the high and selective CO_2 uptake of this MOF at low pressure, due to an adequate confined space combining the high density of OH groups on the edge sharing Al chains of octahedra and packed phenyl groups aligned along the inner

walls of the channels. While the exceptional thermal and hydrolytic stability of this MOF was demonstrated, a moderate CO_2 enthalpy of adsorption was deduced of *ca*. 40 kJ mol^{-1}, comparable to benchmark MOF physisorbents, which is an asset for its potential use for CO_2 capture applications. Besides, a kilogram-scale synthesis protocol for MIL-120(Al)-AP was obtained with a high STY, using inexpensive commercially available precursors via a green and cheap ambient pressure route. MIL-120(Al)-AP was also shaped with bentonite and silica which provided good mechanic strength while keeping the sorption performances. Then, the efficient CO_2 adsorption performance of this MOF was further confirmed thanks to dynamic column breakthrough experiments, while fundamental *operando* IR studies suggested, to some extent, the potential to operate in humid conditions through a kinetic separation process. Since MIL-120(Al)-AP is made from cost-effective raw materials with a sustainable scale-up in water, a techno-economic evaluation of the total industrial production cost indicated a 12.94 $/kg at the kton-scale, among the lowest ever reported for MOFs. This, in addition to its adsorption characteristics, easy synthesis, low cost and robustness, suggests that MIL-120(Al)-AP lies as one of the scarce MOFs that meet the necessary criteria for its practical use in real-life post-combustion carbon capture processes. In particular, this material could be interesting for TSA processes where regeneration could be completed in the presence of humidity at 50 °C, a low temperature that is relatively easy to obtain from waste heat from industrial processes such as cement or steel production.

Authors information

Corresponding Authors: Guillaume Maurin, Georges Mouchaham and Christian Serre

E-mails: guillaume.maurin1@umotpellier.fr; georges.mouchaham@ens.psl.eu; christian.serre@ens.psl.eu

Author Contributions. The manuscript was written through the contributions of all authors. B.C. performed towards the synthesis and the basic characterization. D.F. and G.M. contributed towards the theoretical studies. I.D. and C.M. performed the *in situ* SRPD measurements, I.D. performed the crystal structure data analysis. S.N. contributed to the gas and vapor sorption isotherms measurements and the analysis associated data. R.P. and D.C. contributed towards the scale-up and shaping studies

with the help and the guidance of F.N., I.C. and P.F. performed solid state multinuclear (^{1}H, ^{13}C, and ^{27}Al) NMR (ssNMR) Magic Angle Spinning (MAS) studies. N.G.M., A.V. and M.D. performed, analyzed and discussed the IR experiments. N.H. and G.D.W. performed adsorption isotherm and the dynamic breakthrough curve measurements, calculated IAST selectivity and isosteric enthalpy of adsorption and contributed towards identifying the potential in CO_2 capture processes. M.B., A.A.M. and M.P. investigated the techno-economic analysis. G.M. and C.S. supervised the work and contributed towards the overall concept.

Aknowledgements. The Authors acknowledge the European Union's Horizon 2020 research and innovation programme under grant agreement No. 831975 (MOF4AIR project) for providing financial support. M.P., M.B. and A.A.M. acknowledge Portuguese FCT/MCTES, and when applicable ERDF under the PT2020 partnership agreement, for the funding of the projects UIDB/04028/2020 and UIDP/04028/2020 (CERENA) and UIDB/50011/2020, UIDP/50011/2020 and LA/P/0006/2020 (CICECO). The computational work was performed using HPC resources from GENCI-CINES (Grant A0140907613). B.C. is grateful for support from a CSC grant (grant number 201804910475). M.B. gratefully acknowledges FCT for the PhD grant ref. SFRH/BD/147239/2019. The authors are thankful to the Swiss-Norwegian Beamlines (SNBL) staff at the European Synchrotron Radiation Facility (ESRF). We thank Dr. Antoine Tissot for his help in remeasuring SCXRD structure of MIL-120(Al)-HP. M. Masheer Ul-Haq is aknowledged for his contribution to the synthesis part.

Notes: The authors declare no competing interest.

References

[1] N. Mac Dowell, P. S. Fennell, N. Shah, G. C. Maitland, *Nature Climate Change* **2017**, 7, 243.

[2] A. Samanta, A. Zhao, G. K. Shimizu, P. Sarkar, R. Gupta, *Industrial & Engineering Chemistry Research* **2012**, 51, 1438.

[3] a)B. Dutcher, M. Fan, A. G. Russell, *ACS applied materials & interfaces* **2015**, 7, 2137; b)M. Wang, A. S. Joel, C. Ramshaw, D. Eimer, N. M. Musa, *Applied Energy* **2015**, 158, 275.

[4] J. Arakawa, S. Okuno, K. Takano, Y. Yamanaka, T. Matsuyama, P. Feron, A. Cottrell, A. Cousins, S. Huang, R. Davies, P. Sertori, *Energy Procedia* **2017**, 114, 1061.

[5] a)Q. Hou, Y. Wu, S. Zhou, Y. Wei, J. Caro, H. Wang, *Angewandte Chemie International Edition* **2019**, 58, 327; b)L. Zou, Y. Sun, S. Che, X. Yang, X. Wang, M. Bosch, Q. Wang, H. Li, M. Smith, S. Yuan, *Advanced materials* **2017**, 29, 1700229.

[6] a)Y. Zhou, J. Zhang, L. Wang, X. Cui, X. Liu, S. S. Wong, H. An, N. Yan, J. Xie, C. Yu, P. Zhang, Y. Du, S. Xi, L. Zheng, X. Cao, Y. Wu, Y. Wang, C. Wang, H. Wen, L. Chen, H. Xing, J. Wang, *Science* **2021**, 373, 315; b)S. J. Datta, C. Khumnoon, Z. H. Lee, W. K. Moon, S. Docao, T. H. Nguyen, I. C. Hwang, D. Moon, P. Oleynikov, O. Terasaki, K. B. Yoon, *Science* **2015**, 350, 302.

[7] a)G. Qi, Y. Wang, L. Estevez, X. Duan, N. Anako, A.-H. A. Park, W. Li, C. W. Jones, E. P. Giannelis, *Energy & Environmental Science* **2011**, 4, 444; b)Y. Zeng, R. Zou, Y. Zhao, *Advanced Materials* **2016**, 28, 2855; c)J. M. Kolle, M. Fayaz, A. Sayari, *Chemical Reviews* **2021**, 121, 7280.

[8] E. J. Kim, R. L. Siegelman, H. Z. Jiang, A. C. Forse, J.-H. Lee, J. D. Martell, P. J. Milner, J. M. Falkowski, J. B. Neaton, J. A. Reimer, *Science* **2020**, 369, 392.

[9] R. L. Siegelman, E. J. Kim, J. R. Long, *Nature Materials* **2021**, 20, 1060.

[10] a)D. M. D'Alessandro, B. Smit, J. R. Long, *Angewandte Chemie International Edition* **2010**, 49, 6058; b)X. Zhao, Y. Wang, D.-S. Li, X. Bu, P. Feng, *Advanced Materials* **2018**, 30, 1705189; c)M. N. Dods, S. C. Weston, J. R. Long, *Advanced Materials* **2022**, 34, 2204277.

[11] J.-B. Lin, T. T. Nguyen, R. Vaidhyanathan, J. Burner, J. M. Taylor, H. Durekova, F. Akhtar, R. K. Mah, O. Ghaffari-Nik, S. Marx, *Science* **2021**, 374, 1464.

[12] a)S. Mukherjee, N. Sikdar, D. O'Nolan, D. M. Franz, V. Gascón, A. Kumar, N. Kumar, H. S. Scott, D. G. Madden, P. E. Kruger, *Science advances* **2019**, 5, eaax9171; b)S. Ullah, K. Tan, D. Sensharma, N. Kumar, S. Mukherjee, A. A. Bezrukov, J. Li, M. J. Zaworotko, T. Thonhauser, *Angewandte Chemie* **2022**, e202206613; c)P. Nugent, Y. Belmabkhout, S. D. Burd, A. J. Cairns, R. Luebke, K. Forrest, T. Pham, S. Ma, B. Space, L. Wojtas, M. Eddaoudi, M. J. Zaworotko, *Nature* **2013**, 495, 80; d)P. M. Bhatt, Y. Belmabkhout, A. Cadiau, K. Adil, O. Shekhah, A. Shkurenko, L. J. Barbour, M. Eddaoudi, *Journal of the American Chemical Society* **2016**, 138, 9301.

[13] a)M. Gaab, N. Trukhan, S. Maurer, R. Gummaraju, U. Müller, *Microporous and Mesoporous Materials* **2012**, 157, 131; b)M. Rubio-Martinez, T. D. Hadley, M. P. Batten, K. Constanti-Carey, T. Barton, D. Marley, A. Mönch, K. S. Lim, M. R. Hill, *ChemSusChem* **2016**, 9, 938.

[14] Z. Zheng, H. L. Nguyen, N. Hanikel, K. K.-Y. Li, Z. Zhou, T. Ma, O. M. Yaghi, *Nature Protocols* **2023**, 18, 136.

[15] a)A. Permyakova, O. Skrylnyk, E. Courbon, M. Affram, S. Wang, U. H. Lee, A. H. Valekar, F. Nouar, G. Mouchaham, T. Devic, G. De Weireld, J.-S. Chang, N. Steunou, M. Frère, C. Serre, *ChemSusChem* **2017**, 10, 1419; b)E. Hastürk, S.-P. Höfert, B. Topalli, C. Schlüsener, C. Janiak, *Microporous and Mesoporous Materials* **2020**, 295, 109907; c)E. Gkaniatsou, C. Chen, F. S. Cui, X. Zhu, P. Sapin, F. Nouar, C. Boissière, C. N. Markides, J. Hensen, C. Serre, *Cell Reports Physical Science* **2022**, 3, 100730.

[16] T. Loiseau, G. Ferey, C. Volkringer, F. Taulelle, M. Haouas, PCT/FR2009/052208 Patent, **2010**.

[17] M. I. Severino, E. Gkaniatsou, F. Nouar, M. L. Pinto, C. Serre, *Faraday Discussions* **2021**, 231, 326.

[18] C. Volkringer, T. Loiseau, M. Haouas, F. Taulelle, D. Popov, M. Burghammer, C. Riekel, C. Zlotea, F. Cuevas, M. Latroche, *Chemistry of Materials* **2009**, 21, 5783.

[19] D. Cunha, M. Ben Yahia, S. Hall, S. R. Miller, H. Chevreau, E. Elkaïm, G. Maurin, P. Horcajada, C. Serre, *Chemistry of Materials* **2013**, 25, 2767.

[20] P. G. Boyd, A. Chidambaram, E. García-Díez, C. P. Ireland, T. D. Daff, R. Bounds, A. Gładysiak, P. Schouwink, S. M. Moosavi, M. M. Maroto-Valer, J. A.

Reimer, J. A. R. Navarro, T. K. Woo, S. Garcia, K. C. Stylianou, B. Smit, *Nature* **2019**, 576, 253.

[21] C. Serre, G. Mouchaham, B. Chen, PCT/FR2022/051468 Patent WO2023/002141A1, **01/2023**.

[22] R. P. Loughran, T. Hurley, A. Gładysiak, A. Chidambaram, K. Khivantsev, E. D. Walter, T. R. Graham, P. Reardon, J. Szanyi, D. B. Fast, Q. R. S. Miller, A.-H. A. Park, K. C. Stylianou, *Cell Reports Physical Science* **2023**, 4, 101470.

[23] C. Volkringer, T. Loiseau, N. Guillou, G. Férey, M. Haouas, F. Taulelle, E. Elkaim, N. Stock, *Inorganic chemistry* **2010**, 49, 9852.

[24] D. Britt, H. Furukawa, B. Wang, T. G. Glover, O. M. Yaghi, *Proceedings of the National Academy of Sciences* **2009**, 106, 20637.

[25] A. Masala, J. G. Vitillo, G. Mondino, C. A. Grande, R. Blom, M. Manzoli, M. Marshall, S. Bordiga, *ACS applied materials & interfaces* **2017**, 9, 455.

[26] H. A. Evans, D. Mullangi, Z. Deng, Y. Wang, S. B. Peh, F. Wei, J. Wang, C. M. Brown, D. Zhao, P. Canepa, *Science Advances* **2022**, 8, eade1473.

[27] O. Shekhah, Y. Belmabkhout, Z. Chen, V. Guillerm, A. Cairns, K. Adil, M. Eddaoudi, *Nature communications* **2014**, 5, 1.

[28] C. Chen, X. Feng, Q. Zhu, R. Dong, R. Yang, Y. Cheng, C. He, *Inorganic chemistry* **2019**, 58, 2717.

[29] F. Su, C. Lu, *Energy & Environmental Science* **2012**, 5, 9021.

[30] A. Anson, C. C. H. Lin, S. M. Kuznicki, J. A. Sawada, *Chemical Engineering Science* **2009**, 64, 3683.

[31] a)C. Cleeton, F. L. de Oliveira, R. F. Neumann, A. H. Farmahini, B. Luan, M. Steiner, L. Sarkisov, *Energy & Environmental Science* **2023**; b)T. T. T. Nguyen, J.-B. Lin, G. K. H. Shimizu, A. Rajendran, *Chemical Engineering Journal* **2022**, 442, 136263.

[32] a)M. J. Thompson, C. L. Hobday, I. Senkovska, V. Bon, S. Ehrling, M. Maliuta, S. Kaskel, T. Düren, *Journal of Materials Chemistry A* **2020**, 8, 22703; b)I. Senkovska, V. Bon, L. Abylgazina, M. Mendt, J. Berger, G. Kieslich, P. Petkov, J. Luiz Fiorio, J.-O. Joswig, T. Heine, L. Schaper, C. Bachetzky, R. Schmid, R. A. Fischer, A. Pöppl, E. Brunner, S. Kaskel, *Angewandte Chemie International Edition* **2023**, 62, e202218076.

[33] J. Rodríguez-Carvajal, *Physica B: Condensed Matter* **1993**, 192, 55.

[34] V. Favre-Nicolin, R. Černý, *Journal of Applied Crystallography* **2002**, 35, 734.

[35] H. M. Lee, I. S. Youn, M. Saleh, J. W. Lee, K. S. Kim, *Physical Chemistry Chemical Physics* **2015**, 17, 10925.

[36] D. Lenzen, J. Zhao, S.-J. Ernst, M. Wahiduzzaman, A. Ken Inge, D. Fröhlich, H. Xu, H.-J. Bart, C. Janiak, S. Henninger, G. Maurin, X. Zou, N. Stock, *Nature Communications* **2019**, 10, 3025.

[37] A. Permyakova, O. Skrylnyk, E. Courbon, M. Affram, S. Wang, U.-H. Lee, A. H. Valekar, F. Nouar, G. Mouchaham, T. Devic, G. De Weireld, J.-S. Chang, N. Steunou, M. Frère, C. Serre, *ChemSusChem* **2017**, 10, 1419.

[38] Nouar farid, Serre christian, Pinto ML, Severino MI, Pimenta V, F. C., *ChemRxiv. Cambridge: Cambridge Open Engage* **2023**.

[39] *World Energy Outlook 2022 (International Energy Agency)* **2022**.

[40] in *Chemical Engineering Plant Cost Index*, https://www.chemengonline.com/pci-home.